 ©2008 Kvantovaya Elektronika and Turpion Ltd

PACS numbers: 42.60.By; 42.60.Jf; 42.65.Re
DOI: 10.1070/QE2008v038n11ABEH013833

Third-order correlator for measuring the time profile of petawatt laser pulses

V.N. Ginzburg, N.V. Didenko, A.V. Konyashchenko, V.V. Lozhkarev, G.A. Luchinin, G.A. Lutsenko, S.Yu. Mironov, E.A. Khazanov, I.V. Yakovlev

***Abstract*. A third-order correlator with a single-shot time window and a full dynamic range of 10^8 is developed. The time contrast of radiation from the front-end system of a petawatt femtosecond laser complex measured with the correlator within time windows ± 1 ps and ± 100 ps was 10^4 and more than 10^8, respectively. Based on the theoretical analysis of the cross-correlator operation, a number of requirements providing the optimal functioning of the cross-correlator are found. The reasons restricting the technical parameters of the correlator are discussed.**

Keywords: *time contrast, third-order correlator, single-shot detection, femtosecond pulses.*

1. Introduction

Due to a considerable advance in the development of petawatt laser complexes, the record intensity of focused laser radiation obtained at present achieves 10^{22} W cm^{-2} [1]. Multipetawatt laser systems are being developed in a number of laboratories worldwide. A unique petawatt femtosecond laser complex developed at the Institute of Applied Physics, RAS uses the parametric amplification of chirped pulses to obtain peak pulse powers up to 0.56 PW [2].

Superhigh-power laser radiation is used in experimental studies of the behaviour of matter in a strong electromagnetic field, the acceleration of electrons and other elementary particles [3, 4]. Such experiments require the use of highly contrast laser pulses.

The reduction of the time contrast of superhigh-power laser pulses is caused by a number of reasons related to the method of generation of radiation. In particular, the main reasons in laser complexes with parametric amplification of chirped pulses are parametric superluminescence, the uncompensated higher-order residual dispersion, the spectral restriction by the diffraction gratings of a stretcher and a compressor, and random phase noise caused by the inhomogeneities of optical elements [5]. The reduction of the contrast of femtosecond pulses caused by these reasons is manifested at different time intervals Δt measured from the main pulse maximum. In this connection the total time interval is divided into three parts corresponding to the main pulse and the regions of the near ($\Delta t = \pm 1$ ps) and far ($t = 500$ ps and more) contrasts. The value of the near contrast of radiation of laser systems with amplification of chirped pulses is the criterion for matching a stretcher and a compressor. The far contrast level plays a significant role in experimental studies of the interaction of superhigh-power laser pulses with matter. The presence of a 10^{12}-W cm^{-2} prepulse in this interval leads to the undesirable production of a plasma before the arrival of the main pulse. Therefore, the dynamic measurement range should be no less than $10^{10} - 10^{12}$.

A specific feature of high-power laser systems is the single-pulse operation regime. Therefore, the measurement should be performed during one pulse within the time window, which allows one to obtain information on the laser pulse profile in the interval of duration of a few picoseconds.

By using indirect methods based on nonlinear-optical transformations (generation of harmonics, frequency mixing, parametric amplification), it is possible to achieve the required characteristics of devices for measuring the time intensity distributions of high-power laser radiation. The time intensity profiles are measured with second- and third-order correlators. Conventional second-order correlators have two considerable disadvantages: they cannot distinguish prepulses from postpulses and their dynamic range does not exceed 10^8 [4, 6]. Third-order correlators based on the generation of radiation at the second and third harmonics eliminate these problems and provide the dynamic range up to 10^{10} [3, 4, 7, 8].

In this paper, we considered the operation principle of a third-order correlator with a single-shot time window, the constructive features of a contrast-meter and factors limiting its dynamic range. The results of measurements of the time profile of radiation of the front-end system of a petawatt laser complex were also discussed [2].

V.N. Ginzburg, V.V. Lozhkarev, G.A. Luchinin, S.Yu. Mironov, E.A. Khazanov, I.V. Yakovlev Institue of Applied Physics, Russian Academy of Sciences, ul. Ul'yanova 46, 603950 Nizhnii Novgorod, Russia; e-mail: khazanov@appl.sci.-nnov.ru;
A.V. Konyashchenko, G.A. Lutsenko P.N. Lebedev Physics Institute, Russian Academy of Sciences, Leninsky prosp. 53, 119991 Moscow, Russia; Avesta-Project Limited Liability Company, ul. Solnechnaya 12, 142190 Troitsk, Moscow region, Russia;
N.V. Didenko Avesta-Project Limited Liability Company, ul. Solnechnaya 12, 142190 Troitsk, Moscow region, Russia

Received 28 December 2007; revision received 11 April 2008
Kvantovaya Elektronika **38** (11) 1027 – 1032 (2008)
Translated by M.N. Sapozhnikov

2. Operation principle of a third-order single-shot time window correlator

The method is based on obtaining information on the time shape of a pulse from the spatial distribution of the radiation energy density at the third-harmonic (TH) frequency, which is detected with a CCD array (Fig. 1). The method is a modification of the well-known principle of transformation of the time profile of a radiation pulse to the spatial profile, which is used in second-order correlators for single-shot measurements [9, 10].

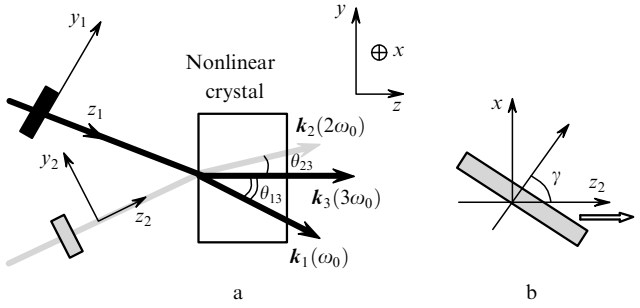

Figure 1. Scheme of the sum-frequency radiation generation (side view) (a) and the top view (along the y_2 axis) of the SH pulse (b). Grey and black rectangles are areas filled with pulses.

The third-harmonic radiation is generated during non-collinear interaction of the radiation under study and second-harmonic (SH) radiation, which is used as the reference radiation.

The noise level in the reference pulse can be reduced by generating the SH in the unsaturated quasi-static regime. To do this, the length L_{SHG} of the nonlinear element of a SH generator should be smaller than the nonlinear length L_{nl} and the length L_{gr} of the group-velocity mismatch of pulses:

$$L_{\mathrm{SHG}} < L_{\mathrm{nl}} = \left(\frac{4\pi\omega_0^2 d_{\mathrm{eff}}}{k_1 c^2} E_1\right)^{-1}, \quad \frac{L_{\mathrm{SHG}}\alpha}{T_1} = \frac{L_{\mathrm{SHG}}}{L_{\mathrm{gr}}} \ll 1, \quad (1)$$

where E_1 is the field amplitude at the nonlinear-element input; d_{eff} is the effective nonlinearity; ω_0, k_1, and T_1 are the central frequency, wave number, and duration of a tested signal; and $\alpha = 1/u_2 - 1/u_1$ is the mismatch of group velocities $u_1(\omega_0)$ and $u_2(2\omega_0)$.

The tilt of the front of the SH radiation allows one to look through the time distribution of the radiation pulse during one realisation. The time-window width depends on the front tilt γ (Fig. 1). A third-harmonic signal measured in an ideal third-order correlator represents the cross section of the correlation intensity function $I(t)$ of radiation being tested:

$$K_{\mathrm{a}}(\tau) = \frac{\int_{-\infty}^{\infty} I(t) I^2(t-\tau)\mathrm{d}t}{\int_{-\infty}^{\infty} I^3(t)\mathrm{d}t}. \quad (2)$$

Because expression (2) contains only signal $I(t)$, we will call the function $K_{\mathrm{a}}(\tau)$ the third-order intensity autocorrelation function.

The time window position can be changed by using a delay line to vary the instant of the pulse arrival (with respect to the SH pulse) on the nonlinear element of a third-harmonic generator (THG) in the range ± 500 ps.

3. Measurement of the third-order intensity autocorrelation function

To increase the TH generation efficiency, the tested radiation and its SH are focused by cylindrical lenses along the y axis on a nonlinear crystal of the THG (Fig. 1). The electric field strengths are described by expressions

$$E_1 = A_1\left(t - \frac{z\cos\theta_{13} - y\sin\theta_{13}}{u_1}\right) \times \exp\left[-\frac{x^2}{R_x^2} - \frac{(y\cos\theta_{13} + z\sin\theta_{13})^2}{R_y^2}\right] \times \exp[-\mathrm{i}\omega_0 t + \mathrm{i}k_1(z\cos\theta_{13} - y\sin\theta_{13})],$$

$$E_2 = A_2\left(t - \frac{z\cos\theta_{23} + y\sin\theta_{23}}{u_2} - \frac{x\tan\gamma}{u_2}\right) \times \exp\left[-\frac{x^2}{R_x^2} - \frac{(y\cos\theta_{23} - z\sin\theta_{23})^2}{R_y^2}\right] \times \exp[-\mathrm{i}2\omega_0 t + \mathrm{i}k_2(z\cos\theta_{23} + y\sin\theta_{23})],$$

where $A_1(t)$ and $A_2(t)$ are the time envelopes of signals at central frequencies ω_0 and $2\omega_0$; θ_{13} and θ_{23} are the angles between the wave vectors $\boldsymbol{k}_1(\omega_0)$, $\boldsymbol{k}_2(2\omega_0)$ and the axis z, respectively (Fig. 1); R_x and R_y are the characteristic sizes of the laser beam focused by a cylindrical lens on the THG along the x and y axes, respectively ($R_x \gg R_y$). The electric field strengths are written for the Gaussian profile of the transverse field distribution.

The field strength at the TH frequency at the output of the nonlinear crystal generated in the unsaturated regime under phase matching conditions for central frequencies $[\boldsymbol{k}_1(\omega_0) + \boldsymbol{k}_2(2\omega_0) = \boldsymbol{k}_3(3\omega_0)]$ can be found similarly to [11]:

$$E_3 = -\mathrm{i}\gamma_3 \int_0^{L_{\mathrm{THG}}} A_1\left[t - \frac{L_{\mathrm{THG}}}{u_3} + \frac{1}{u_3}\left(1 - \frac{u_3\cos\theta_{13}}{u_1}\right)\xi + \frac{y\sin\theta_{13}}{u_1}\right] A_2\left[t - \frac{L_{\mathrm{THG}}}{u_3} + \frac{1}{u_3}\left(1 - \frac{u_3\cos\theta_{23}}{u_2}\right)\xi - \frac{y\sin\theta_{23}}{u_2} - \frac{x\tan\gamma}{u_2}\right] F(x,y,\xi)\mathrm{d}\xi, \quad (3)$$

where L_{THG} is the length of the nonlinear crystal of the THG; $\gamma_3 = (4\pi d_{\mathrm{eff}}\omega_3^2)/(k_3 c^2)$ is the nonlinear coupling coefficient of the waves; $u_3(3\omega_0)$ is the group velocity; and

$$F(x,y,\xi) = \exp\left[-\frac{2x^2}{R_x^2} - \left(\frac{y\cos\theta_{13}}{R_y} + \frac{\xi\sin\theta_{13}}{R_y}\right)^2 - \left(\frac{y\cos\theta_{23}}{R_y} - \frac{\xi\sin\theta_{23}}{R_y}\right)^2\right]$$

is the transverse field distribution.

The expression for the radiation field strength at the TH frequency can be considerably simplified if the conditions

$$p_1 = \left| \frac{L_{\mathrm{THG}}}{u_3 T} \left(1 - \frac{u_3 \cos\theta_{13}}{u_1} \right) \right| < 1,$$
$$p_2 = \left| \frac{L_{\mathrm{THG}}}{u_3 T} \left(1 - \frac{u_3 \cos\theta_{23}}{u_2} \right) \right| < 1 \qquad (4)$$

are fulfilled, where T is the characteristic time scale of radiation. The parameters p_1 and p_2 determine the group velocity mismatch over the crystal length. If these parameters are small, the transverse distribution of the TH radiation energy density can be written in the form

$$\tilde{W}_3(x, y, \tau) \propto \left[\int_{-\infty}^{\infty} A_1^2(t) A_2^2(t-\tau) \mathrm{d}t \right]$$
$$\times F^2(x, y, \xi = 0) \propto K_{\mathrm{a}}(\tau), \qquad (5)$$

where $\tau = [x \tan\gamma + y(\sin\theta_{13} + \sin\theta_{23})]/u$; $u = u_1 = u_2$.

Thus, the radiation energy density distribution measured at the sum frequency [when thin crystals are used (4)] represents the third-order intensity autocorrelation function (2) of the tested signal. The expression for the parameter τ consists of two terms. The first one is related to the tilt of the radiation intensity front at the SH frequency and is necessary to form a time window, while the second one is caused by the noncollinear interaction of the waves.

The pulse intensity profile measured in experiments differs from the real pulse profile. This is explained, at least by two reasons. First, radiation emitted by a femtosecond laser complex contains a broad luminescence noise along with the main pulse and its possible precursors. The description of the conversion of this noise to the TH signal within the framework of our model would be incorrect because its spectral width exceeds the spectral widths of phase matching upon frequency doubling and summation. In this case, nonlinear crystals operate as frequency filters, which reduce the efficiency of the noise-to-signal conversion at the sum frequency and restrict the time resolution of the device. The second reason is the mathematical difference between the contrast function $K(\tau) = I(\tau)/I(0)$ and the third-order intensity autocorrelation function (2). We will consider the influence of this factor on the measurement accuracy in the next section by the example of the model problem of detecting prepulses of the main radiation.

4. Relation between the correlation function and contrast

We assume that the main pulse of the tested signal, its precursor, and SH pulse all have Gaussian time profiles (Fig. 2). The influence of the main pulse of the tested signal on the frequency summation process will be neglected. This is possible, for example, when the prepulse is located far away from the main pulse. Then, the intensities of the tested radiation $I(t)$ and radiation at the SH frequency $I_2(t)$ are described by the expressions

$$I(t) = I_{10} \exp\left[-4 \ln 2 \left(\frac{t}{T} \right)^2 \right]$$
$$+ K(\tau) I_{10} \exp\left[-4 \ln 2 \left(\frac{t-\tau}{T_{\mathrm{p}}} \right)^2 \right],$$
$$I_2(t) = I_{20} \exp\left[-4 \ln 2 \left(\frac{t}{T_2} \right)^2 \right],$$

where T_{p} and T_2 are the durations of the prepulse and SH pulse, respectively. By using the approximation $|\tau| \gg T, T_{\mathrm{p}}, T_2$, and expression (2), we obtain

$$K_{\mathrm{a}}(\tau) = \frac{K(\tau) \int_{-\infty}^{\infty} \exp\left\{ -4 \ln 2 \left[\frac{(t-\tau)^2}{T_{\mathrm{p}}^2} + \frac{(t-\tau)^2}{T_2^2} \right] \right\} \mathrm{d}t}{\int_{-\infty}^{\infty} \exp\left[-4 \ln 2 \left(\frac{t^2}{T^2} + \frac{t^2}{T_2^2} \right) \right] \mathrm{d}t}. \qquad (6)$$

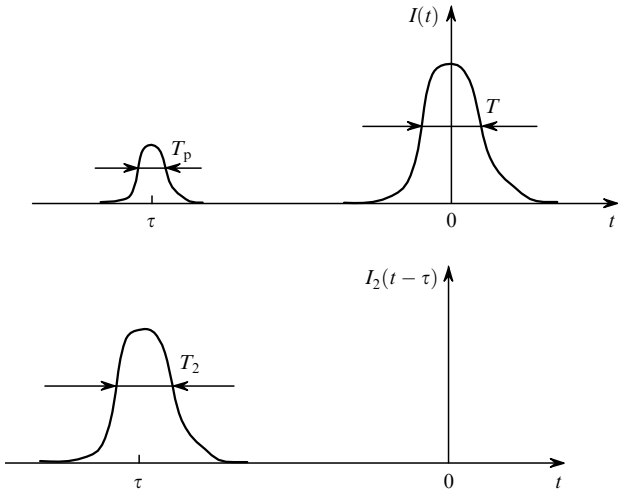

Figure 2. Measurement of the prepulse contrast. The SH radiation pulse is made coincident in time with its precursor.

Expression (6) can be simplified and the ratio of the measured (K_{a}) and real (K) contrasts will take the form

$$\frac{K_{\mathrm{a}}(T_{\mathrm{p}}/T, \chi)}{K(T_{\mathrm{p}}/T)} = \frac{1}{\chi} \left[\frac{1+\chi}{1+\chi^2 (T/T_{\mathrm{p}})^2} \right]^{1/2}, \qquad (7)$$

where $\chi = T_2/T$.

In the case of second harmonic generation (SH) in the quasi-static regime without saturation, the parameter $\chi = 1/\sqrt{2}$, while in the strongly saturated regime, $\chi \sim 1$ (for a Gaussian beam under study). Figure 3 presents the typical dependences of $K_{\mathrm{a}}(T_{\mathrm{p}}/T, \chi)/K$ on the prepulse duration.

Thus, the contrast measured within the framework of the problem under study is virtually independent of the prepulse duration and in the case of the linear SH generation regime, it exceeds the real value by no more than 10 %. For contrast meters with a total dynamic range of 10^8, such an error is insignificant.

5. Experimental results

Figure 4 presents the optical scheme of the developed contrast meter. The second harmonic radiation was generated in a KDP crystal of length 0.5 mm. For radiation

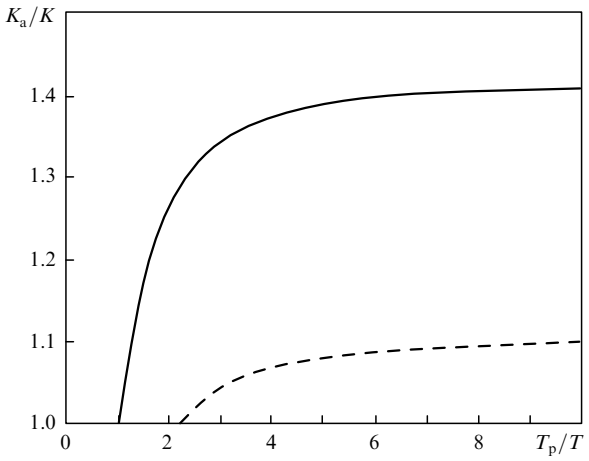

Figure 3. Dependences of K_a/K on the prepulse duration T_p for $\chi = 1$ (solid curve) and $1/\sqrt{2}$ (dashed curve).

with the central wavelength $\lambda_0 = 910$ nm, the (oo – e) phase-matching angle measured from the optical axis was 42°. According to our estimates, the duration of a tested pulse propagated through the nonlinear crystal increased by no more than 1 % from its initial value ~ 70 fs.

The third harmonic radiation was generated in a BBO crystal of length 0.1 mm. The internal angle between vectors $\boldsymbol{k}_1$ and $\boldsymbol{k}_2$ was 5°, the type I (oo – e) phase-matching angle for the direction of the wave vector $\boldsymbol{k}_3$ of third harmonic radiation was $38°2'$. The typical spectral phase-matching width for the mixing crystal was ~ 15 nm for the tested signal at 910 nm [12]. The width of the luminescence band of the amplifying parametric path was 100 nm [13].

Information on the time intensity profile of tested radiation is contained in the spatial distribution of the TH signal energy density. The fundamental and SH radiations are focused by cylindrical lenses on the mixer to increase the TH generation efficiency. Spherical lenses transfer images from the TH generator to a CCD array (Fig. 5). The spatial distributions of the energy density of the fundamental radiation and its second and third harmonics are measured. Integration is performed over the y

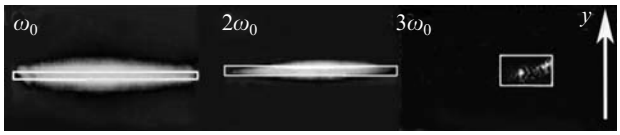

Figure 5. Energy density distributions for different harmonics on the CCD array.

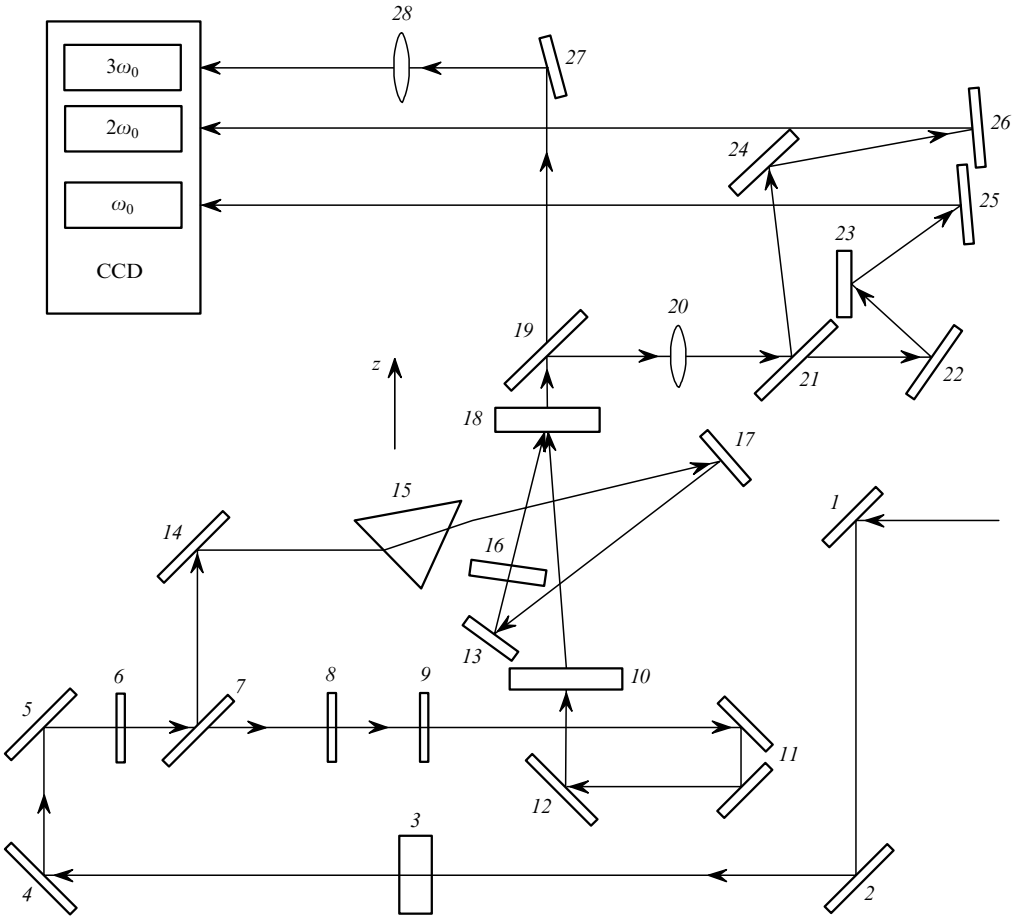

Figure 4. Scheme of a single-shot third-order autocorrelator: (*1*, *2*, *4*, *5*, *12* – *14*, *22* – *27*) mirrors; (*3*) nonlinear KDP crystal; (*6*) attenuator; (*7*, *21*) beamsplitters reflecting the SH radiation and transmitting fundamental radiation; (*8*) glass etalon; (*9*) $\lambda/2$ plate; (*10*, *16*) cylindrical lenses; (*11*) corner reflector; (*15*) prism; (*17*) diffraction grating; (*18*) nonlinear BBO crystal; (*19*) beamsplitter reflecting fundamental and SH radiations and transmitting the TH radiation; (*20*, *28*) lenses.

coordinate of the CCD array. The linearity of SH and TH generations is controlled: the SH energy is $W_2 \sim W_1^2$ and the TH energy is $W_3 \sim W_1 W_2$, where W_1 is the fundamental radiation energy.

The contrast meter provides the measurement of the intensity distribution within the single-shot time window 1 – 10 ps (Fig. 6). The front of the SH radiation intensity is tilted with the help of dispersion elements such as prism (*15*) or diffraction grating (*17*) (Fig. 4).

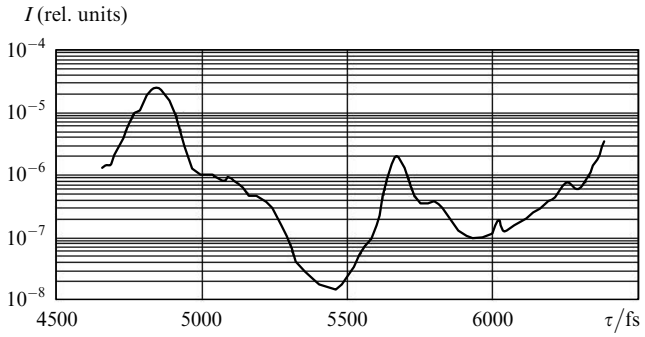

Figure 6. Intensity distribution I in a single-shot time window.

The dynamic range of single-shot measurements with a fixed delay line is determined by the CCD array parameters and is $\sim 10^4$. The total temporal profile of a pulse is obtained by 'gluing' the time windows measured at different delays. In the absence of a delay between the tested pulse and SH signal (in the region of the main maximum), an attenuator reduces maximally the input radiation intensity, while in the case of studying pulse wings, it increases the input pulse energy. We used a diffraction attenuator in our device. The time and amplitude calibrations of the contrast meter were verified by placing a glass etalon into the optical path of fundamental radiation. This resulted in the appearance of additional peaks with known delays in the measured intensity profile.

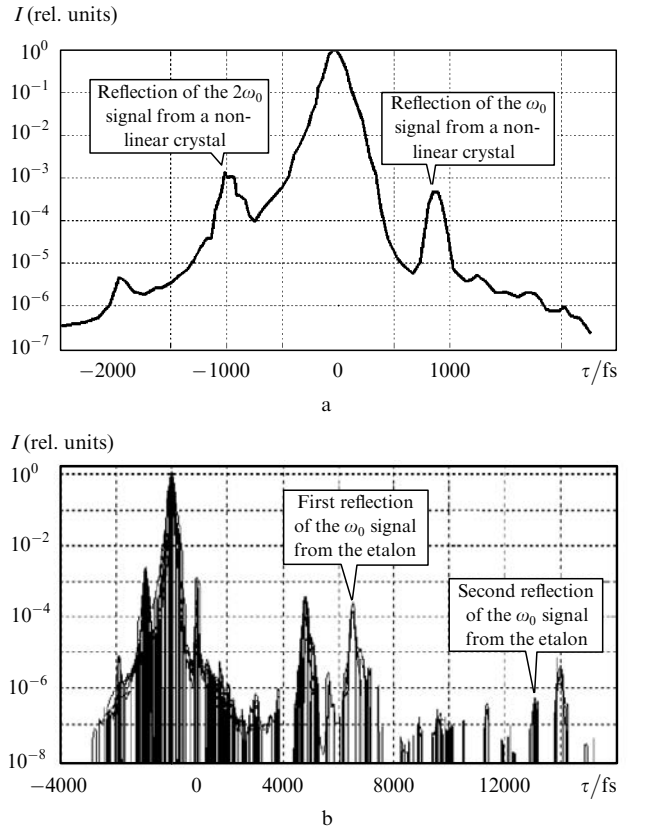

Figure 7. Time intensity profile I for the front-end system of the laser complex: near-contrast region (a) and the intensity profile 'glued' from individual time windows (b) (calibration was performed by using a glass etalon).

The time profile of the radiation intensity of the front-end system of the femtosecond laser complex was measured by using 70-fs, 0.1 – 1 mJ, 910-nm output laser pulses. The laser beam diameter was $D \sim 0.5$ cm. The SH radiation intensity front was tilted by using a prism, the time window width being 2 – 3 ps. Figure 7 shows the radiation intensity profile measured with the contrast meter.

The dispersion broadening of light pulses in optical elements almost does not introduce errors to the contrast measurements if, as in our case, thin nonlinear crystals are used. However, the elongation of the fundamental pulse reduces its peak power, thereby reducing the pulse contrast because the amplified spontaneous radiation background does not change in this case. In a crystal generating the sum-frequency radiation, parasitic TH radiation is present. This radiation restricts the dynamic measurement range by the value 10^8 and, as a result, we have failed to detect the amplified luminescence noise level in the parametric channel (Fig. 7). The near contrast of the pulse was 10^4, which is related, in our opinion, to the higher-order residual dispersion, which was uncompensated upon pulse compression. The additional peaks observed in the time profile at the time delay $\tau = \pm 900$ fs are caused by multiple parasitic reflections in the BBO crystal.

By comparing the pulse duration measured with the contrast meter with pulse durations obtained with the help of the single-shot second-order autocorrelator, we found that the time resolution of the contrast meter was 140 fs.

6. Conclusions

We have developed the third-order correlator for measuring the intensity profile of femtosecond pulses and measured the radiation contrast for the front-end system of the petawatt laser complex. The time resolution of the correlator within the single-shot 2 – 3-ps time window was ~ 140 fs. The total dynamic range achieved upon scanning within ± 100 ps was 10^8. The technical parameters of the correlator can be further improved by eliminating the optical noise of the correlator caused by scattering and parasitic generation of the TH radiation. The use of a diffraction grating for tilting the SH radiation intensity front will considerably increase the single-shot time window, allowing the measurement of the contrast of petawatt radiation pulses.

References

1. Bank S.W., Rousseau P., Planchon T.A., Chvykov V., Kalintchenko G., Maksimchuk A., Mourou G.A., Yanovsky V. *Opt. Lett.*, **29**, 2837 (2004).
2. Freidman G.I., Ginzburg V.N., Katin E.V., Khazanov E.A., Kirsanov A.V., Lozhkarev V.V., Luchinin G.A., Mal'shakov A.N., Martyanov M.A., Palashov O.V., Poteomkin A.K., Sergeev A.M., Shaykin A.A., Yakovlev I.V. *Laser Phys. Lett.*, **4** (6), 421 (2007).

3. Tavella F., Schmid K., Ishii N., Veisz L., Marcinkevicius A., Krausz F. *Appl. Phys. B*, **81**, 753 (2005).
4. Divall E.J., Ross I.N. *Opt. Lett.*, **29** (19), 2273 (2004).
5. Hong K., Hou B., Nees J., Power E., Mourou G. *Appl. Phys. B*, **81**, 447 (2005).
6. Braun A., Rudd J.V., Cheng H., Mourou G., Kopf D., Jung I.D., Weingarten K.J., Keller U. *Opt. Lett.*, **20** (18), 1889 (1995).
7. Osvay K., Ross I., Lister J., Hooker C. *Appl. Phys. B*, **69**, 19 (1999).
8. Belinskii A.V., Silant'eva I.A., Telegin L.S., Chirkin A.S. *Pis'ma Zh. Eksp. Teor. Fiz.*, **10**, 1258 (1984).
9. Brun A., Georges P., Le Saux G., Salin F. *J. Phys. D*, **24**, 1225 (1991).
10. Kazutaka Oba, Pang-Chen Sun, Mazurenko Yu.T., Fainman Y. *Appl. Opt.*, **38** (17), 3810 (1999).
11. Akhmanov S.A., Chirkin A.S., Vysloukh V.A. *Optika femtosekundnykh impul'sov* (Optics of Femtosecond Pulses) (Moscow: Nauka, 1988) pp 49, 127.
12. Dmitriev V.G., Gurzadyan G.G., Nikogosyan D.N. *Handbook of Nonlinear Optical Crystals* (New York, Berlin: Springer, 1999) Vol. 64, p. 44.
13. Ginzburg V.N., Freidman G.I., Katin E.V., Khazanov E.A., Kirsanov A.V., Lozhkarev V.V., Luchinin G.A., Mal'shakov A.N., Martyanov M.A., Palashov O.V., Poteomkin A.K., Sergeev A.M., Shaykin A.A., Yakovlev I.V. *Proc. SPIE Int. Soc. Opt. Eng.*, **5975**, 59750F (2006).